Pinched Hysteresis Loop in Defect-Free Ferroelectric Materials

Bin Xu,[1,*] Charles Paillard,[1,2] Brahim Dkhil,[2] and L. Bellaiche[1]

[1] *Physics Department and Institute for Nanoscience and Engineering, University of Arkansas, Fayetteville, Arkansas 72701, USA*

[2] *Laboratoire SPMS, CentraleSupélec/CNRS UMR8580, Université Paris-Saclay, France*

(Dated: September 28, 2016)

In addition to the single polarization-*versus*-electric field hysteresis loop that is characteristic of ferroelectrics and the double hysteresis loop that is known to occur in antiferroelectrics, a third kind of polarization-*versus*-electric field function has been reported in several systems. This third kind is commonly termed the "pinched" loop due to its unusual shape, and is typically believed to originate from the pinning of domain walls interacting with defects. Here, using an atomistic effective Hamiltonian scheme, we demonstrate that such belief has to be broadened since our simulations also yield pinched loops in defect-free ferroelectric materials, as a result of the occurrence of intermediate modulated phases exhibiting an inhomogeneous dipolar pattern leading to the coexistence of both ferroelectric and antiferroelectric orders.

PACS numbers: 77.80.Dj,77.80.-e,77.80.B-,77.80.bg

The dependency of the electrical polarization $\boldsymbol{P}$ on an applied electric field $\boldsymbol{E}$, in systems possessing electric dipoles, is a fundamental function that is also at the heart of current technologies and future applications. For instance, this function in ferroelectrics (FE) has the form of the single hysteresis loop shown in Fig. 1a and is representative of controlled transitions between two equivalent ferroelectric states having opposite direction for their polarization, therefore allowing this type of materials to be used in memories and logic devices[1, 2]. Similarly, the very specific $\boldsymbol{P}$-*versus*-$\boldsymbol{E}$ function of antiferroelectric (AFE) compounds [3, 4], that is the double hysteresis loop depicted in Fig. 1b and that arises from the existence of field-induced AFE-to-FE and FE-to-AFE transitions, is currently receiving a lot of attention due to its prospect for energy storage applications [5–7]. Note that the double hysteresis loop of Fig. 1b can also happen for temperatures larger than the Curie temperature, T_C, in systems possessing a first-order ferroelectric-to-paraelectric transition such as $BaTiO_3$, as a result of the upward shift of T_C under electric field [8].

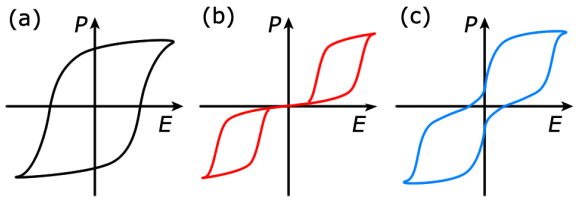

FIG. 1. (Color online) Schematic of three different types of electrical polarization *versus* applied electric field loops. (a) Single loop, as found in ferroelectrics; (b) Double hysteresis loop with zero remnant polarization, as characteristic of AFE compounds; and (c) Pinched hysteresis loop with finite but small remnant polarization.

Surprisingly, in addition to the typical single and double hysteresis loops known to exist in ferroelectrics and antiferroelectrics, a third kind of $\boldsymbol{P}$-$\boldsymbol{E}$ curve has been found in various materials, e.g., $Pb(Zr,Ti)O_3$ [9], $BiFeO_3$ ceramics [10], or $Pb(Yb_{1/2}Nb_{1/2})O_3$-$PbTiO_3$ solid solutions [11]. Such third kind is illustrated in Fig. 1c, and is typically coined "pinched" loop, due to the fact that it can be geometrically constructed from the "pinching" of the single FE hysteresis loop of Fig. 1a at low fields. This pinching therefore leads to a small but finite polarization for zero electric field, unlike the cases of FE (large polarization) and AFE (null polarization) hysteresis loops. It is commonly believed that the existence of pinched loops requires some types of inhomogeneity and structural defects to be present in the material [12], such as domain walls being strongly pinned by defects [9, 10]. However, due to the fact that Fig. 1c can also be geometrically considered as being a linear combination between the hysteresis loops of FE and AFE materials represented in Figs 1a and 1b, respectively, and that these two latter loops are intrinsic in nature, it is legitimate to wonder whether pinched loops can also occur in defect-free systems – as also alluded in Ref. [13]. If that is the case, determining what types of phases could be involved in the pinched loops is also of importance to reveal possibly overlooked mechanisms, especially when realizing that observed pinched loops are sometimes "simply" interpreted to be double (antiferroelectric) hysteresis loops [14, 15] and have been indicated to be associated with large piezoelectric response [13, 14] via a novel mechanism coined "polarization twist" in Ref. [13]. Moreover,"pinched" loops are also known to occur in ferrimagnetic systems [16] and drawing analogy and difference (if any) between ferrimagnets and ferri- or ferro-electrics about the origin of these loops would also be of interest.

Motivated to tackle such issues, we chose to study a rare-earth-substituted $BiFeO_3$ multiferroic solid solution (in this work, $Bi_{1-x}Nd_xFeO_3$ or BNFO), because increasing the rare-earth composition in this system makes the

ground state evolving from a FE (rhombohedral $R3c$) phase to an AFE (orthorhombic $Pnma$) phase [14, 17–21], via the emergence of intermediate states within some compositional range. Interestingly, these intermediate states were predicted to be modulated phases made by nanotwins [22], inside which an antipolar vector can coexist with a (relatively small but finite) spontaneous electrical polarization [23] – therefore allowing a smooth bridging between FE and AFE phases. We demonstrate here that the application of electric fields to these intermediate phases precisely leads to pinched hysteresis loops, as a result of field-induced transitions between these phases and FE states. In other words, the common belief that pinched loops can only occur in systems possessing both domains and defects has to be revisited, and the present study points out to the importance of the inhomogeneous dipolar pattern of these intermediate states to explain the existence of intrinsic pinched loops in ferri- and ferroelectrics [13].

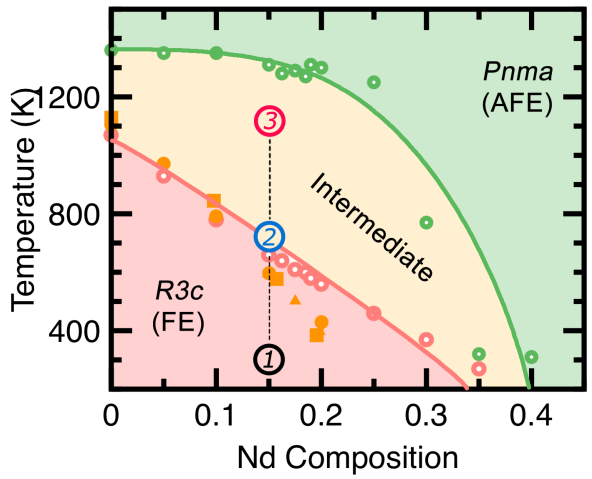

FIG. 2. (Color online) Temperature-composition phase diagram of disordered $Bi_{1-x}Nd_xFeO_3$ sold solutions. The empty symbols denote our predicted phase boundaries at varied compositions, and the solid lines are guides for the eyes based on the calculated data. The solid (orange) symbols denote experimental data [20, 24, 25]. The intermediate phases consist of a series of modulated structures energetically and structurally bridging the $R3c$ and the $Pnma$ phase. The numbers 1, 2 and 3 indicate the three temperatures considered in the present simulations for the Nd composition of 15%.

Here, we adopt the recently developed effective Hamiltonian scheme of Ref. [22] to study disordered BNFO under electric field at finite temperatures. This effective Hamiltonian contains four types of degrees of freedom: 1) the local modes $\{\boldsymbol{u}_i\}$ centered on the A sites (i.e., on Bi or Nd ions), which are proportional to the local electric dipole [26, 27]; 2) the homogeneous $\{\eta_H\}$ and inhomogeneous $\{\eta_I\}$ strain tensors [26, 27]; 3) the pseudo-vectors $\{\boldsymbol{\omega}_i\}$ that characterize the oxygen octahedral tiltings [28]; and 4) the magnetic moments $\{\boldsymbol{m}_i\}$ of the Fe ions. More details about the effective Hamiltonian can be found in the Supplemental Material [29]. The solid solutions are simulated by 12×12×12 supercells (containing 8,640 atoms), in which the Bi and Nd atoms are randomly distributed. The total energy is used within Monte-Carlo simulations employing 40,000 sweeps in order to get converged results.

As a proof of concept, we apply DC external electric fields lying antiparallel or parallel to the pseudo-cubic [111] direction, continuously changing their value from 15 to -15 MV cm^{-1}. We also decided to focus on a single composition, namely 15% of Nd, in BFO because it possesses different types of equilibrium state depending on the temperature, according to our simulations [22] and/or experiments [20, 24, 25]. As a matter of fact and as depicted in Fig. 2, it adopts a ferroelectric rhombohedral $R3c$ state below 660 K *versus* an orthorhombic antiferroelectric $Pnma$ phase above 1300 K, and a family of intermediate complex phases in-between – that were predicted to be nanotwins in Ref. [22] (note that the phase diagram of Fig. 2 is practically constructed by starting from the $R3c$ phase at low temperatures and then heating up the system. As a result and for kinetic reasons, the predicted transition temperatures should be interpreted as upper limits of the phase boundaries, in particular for low temperatures and high Nd compositions – since $R3c$ is metastable for these conditions). As schematized in Fig. 3a, the FE $R3c$ phase has a polarization pointing along a $< 111 >$ direction and oxygen octahedra tilting in anti-phase fashion about the same axis ($a^-a^-a^-$ in Glazer notation [30]). The AFE orthorhombic $Pnma$ phase (Fig. 3b) is characterized by anti-polar distortions along a pseudocubic $< 110 >$ direction, as well as anti-phase oxygen octahedra tiltings about $< 110 >$ and in-phase tiltings about a $< 001 >$ direction ($a^-a^-c^+$ in Glazer notation [30]). The complex phases consist of a series of structures bridging the FE and AFE phases, with complex patterns of Bi/Nd displacements (giving rise to both a spontaneous polarization and an AFE vector) and oxygen octahedral tiltings being modulated along a $< 001 >$ direction, as shown in Fig. 3c. Note that the complex phases have also been predicted to occur in pure BFO, at high temperature or at lower temperature but under hydrostatic pressure [23, 31].

We investigate here three different temperatures, namely, 300, 700 and 1100 K. For the two lowest temperatures, $R3c$ and complex phases with significant polarization are the most stable states under no electric field, respectively. For the third temperature, the most stable states are also made of complex phases but with a negligible spontaneous polarization, therefore allowing us to consider them as AFE state.

Let us now focus on the computed $\boldsymbol{P}$-$\boldsymbol{E}$ curves for these different temperatures. Note that these curves

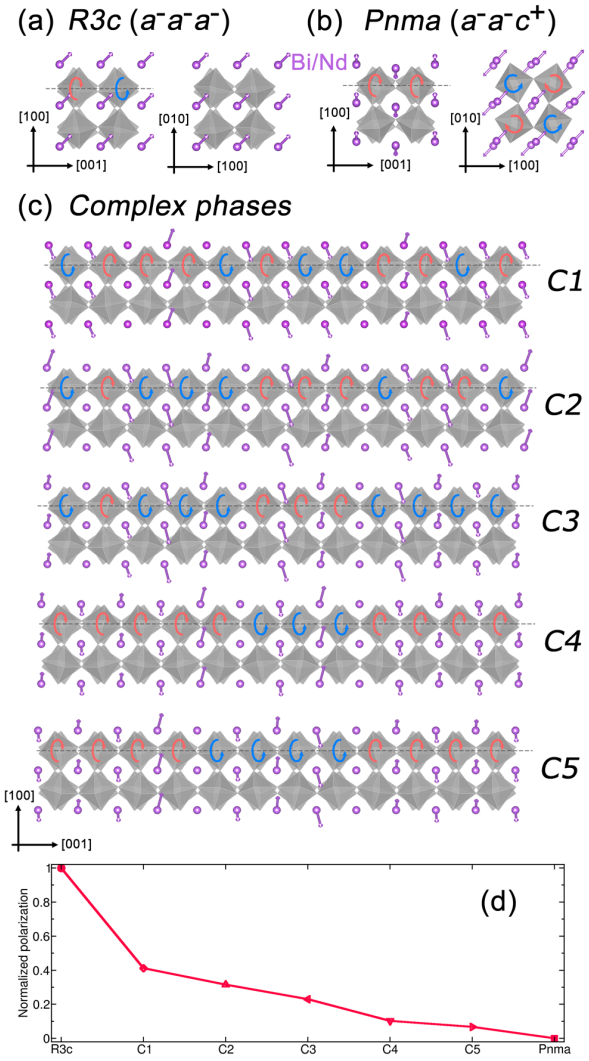

FIG. 3. (Color online) Studied phases of $Bi_{1-x}Nd_xFeO_3$. (a) The ferroelectric *R3c* phase. (b) The antiferroelectric orthorhombic *Pnma* phase. (c) Complex phases with modulation of cation displacements (which results in the formation of a polarization and a AFE vector) and of oxygen octahedral distortions being along the pseudo-cubic [001] direction. To illustrate the structural difference, two opposite tiltings about the [001] axis are denoted by red and blue curled arrows, respectively. The purple arrows on Bi/Nd atoms indicate the local electric dipole, as averaged for each (001) layer. (d) Normalized component of the polarization along the [111] direction of all the occurring phases (the *R3c* phase has a reference polarization of 1 while the polarization of the *Pnma* phase is zero). The VESTA code is used for the visualization [32].

are practically calculated starting from the *R3c* phase at high $\boldsymbol{E}$ and completing the cycle by decreasing and then increasing the $\boldsymbol{E}$-field. For instance, at 300K, Figure 4a reports a single hysteresis loop that is qualitatively very similar to the schematization of Fig. 1a for ferroelectrics. Within this loop, the polarization is switched between *R3c* phases of opposite $\boldsymbol{P}$, at electric fields of about $\pm$ 5 MV cm^{-1}. Note that we also numerically found (not shown here) that during the switching of $\boldsymbol{P}$ (from pseudo-cubic [111] to $[\bar{1}\bar{1}\bar{1}]$ or *vice-versa*), the antiphase octahedral tiltings are not reversed but rather remain about the [111] direction. This can be explained by a specific energetic coupling between local modes and oxygen octahedral tilting pseudo-vectors [33] of the form $u_{i,x}u_{i,y}\omega_{i,x}\omega_{i,y} + u_{i,y}u_{i,z}\omega_{i,y}\omega_{i,z} + u_{i,z}u_{i,x}\omega_{i,z}\omega_{i,x}$, where the x, y and z subscripts denote components along the pseudo-cubic [100], [010] and [001] directions, respectively – since this coupling energy is invariant when the x, y and z components of the local modes (and thus polarization) *all* reverse their sign.

Figure 4c shows the $\boldsymbol{P}$-$\boldsymbol{E}$ curve for a temperature of 1100 K, which yields a double loop that is strikingly similar to the AFE curve displayed in Fig. 1b. In this loop, for zero electric field, the corresponding state is a complex phase (*C4* or *C5*) shown in Fig. 3c, and having a very small polarization (see Fig. 3d). Increasing the field in magnitude then leads to a rather smooth enhancement of the polarization via the evolution of the *C4* or *C5* phase into other complex states displayed in Fig. 3c, namely *C2* or *C3*, before the material undergoes a transition towards *R3c*.

Furthermore, for the temperature of 700 K and as shown in Fig. 4b, the $\boldsymbol{P}$-$\boldsymbol{E}$ curve strongly resembles the pinched loop depicted in Fig. 1c. Starting from the *R3c* state at high field in this loop and progressively reducing the field from 10 to 1 MV cm^{-1}, the structure remains to be *R3c*. Further reducing $\boldsymbol{E}$ to zero then increasing it in the reverse direction induce phase transitions to complex modulated phases in the range of $\boldsymbol{E}$ between 0 and -8 MV cm^{-1}. In particular, for zero field, the polarization neither vanishes as in the AFE loop of Fig. 4c nor is big as in the ferroelectric loop of Fig. 4a, but is rather finite and small – as characteristic of some complex phases (e.g., *C1*). Interestingly, such non-zero but small remnant polarization has indeed been observed in the experimental $\boldsymbol{P}$-$\boldsymbol{E}$ loops [14, 15, 17, 34] of BRFO (R=rare earth) but also of $(Bi_{0.5}Na_{0.5})TiO_3$-$BaTiO_3$ systems [13] that have been recently shown to exhibit long-period modulated phases [35] (as similar to our presently studied intermediate states). Moreover, the projection of the polarization along [111] of our predicted complex phases varies smoothly from positive to negative values (see Fig. 4b), while three different complex phases (*C1*, *C4* and *C5*) occur. Moreover, from $\boldsymbol{E}$=-9 MV cm^{-1} to even large field along $[\bar{1}\bar{1}\bar{1}]$, the *R3c* phase is the most stable phase again. The other half of the $\boldsymbol{P}$-$\boldsymbol{E}$ loop is similar, with *R3c* phase occurring from -10 to 0 MV cm^{-1}, then two complex phases (having significant polarization near zero fields) happens from 1 to 9 MV cm^{-1} before reaching the *R3c* phase again at 10 MV cm^{-1}.

Figure 4b therefore demonstrates that pinched loops can happen when intermediate complex phases, with finite polarization (that is significantly large such as that

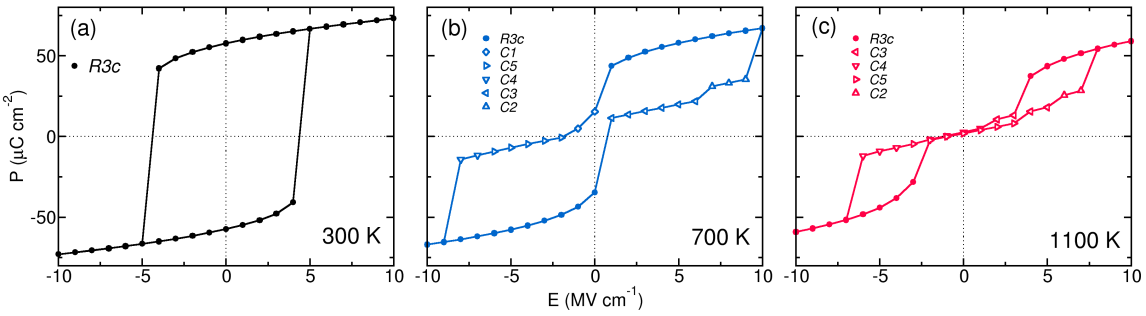

FIG. 4. (Color online) Calculated ***P*-*E*** loops of $Bi_{1-x}Nd_xFeO_3$ having a 15% Nd composition, at three temperatures. (a) 300 K. (b) 700 K. (c) 1100 K. The electric field is applied along the [111] direction, and the displayed polarization is the projected value in this direction. Solid symbols denote the *R*3*c* phase, and open symbols denote complex phases. Arrows indicate how the electric field is varied in the simulated cycle.

in the *C*1 phase) as well as possessing an AFE vector, are involved during the switching from one ferroelectric state with a relatively strong polarization (e.g., *R*3*c*) to another of such ferroelectric state with a reversed polarization. Such finding therefore contrasts with the common belief that pinched loops originate from the existence of multidomains and structural defects [12], such as domain walls being strongly pinned by charged defects [9, 10]. It is worth noting that the Nd substitution of Bi in BNFO plays a very different role than charged defects, such as vacancies or heterovalent impurities/dopants, since Nd and Bi ions have the same valence of +3; therefore, in the present case, there is no pinning effect to the domain walls by extra-dipoles originating from charged defects.

Moreover, the double hysteresis loops having non-zero remnant polarization that have been observed in BRFO [14, 15] and previously thought to originate from the transitions between the AFE *Pnma* phase and the FE *R*3*c* phase (and to a much lesser extend due to domain-wall pinning or aging [14]), are in fact consistent with our Fig. 4b involving intermediate complex phases.

Interestingly, the intermediate modulated phases (Fig. 3c) can also be viewed as coexistence of the AFE *Pnma* and the FE *R*3*c* structures without domain walls. These special structures arise from the fact that the *Pnma* ($a^-a^-c^+$) and *R*3*c* ($a^-a^-a^-$) phases have the same type of anti-phase in-plane tiltings, while along the modulation direction the tiltings can be either in-phase or anti-phase that the pattern is determined by the lowest-energy configuration [36]. Our findings in BNFO can also be understood as being in line with what Lines and Glass proposed for ***P*-*E*** loops with first-order ferroelectic phase transtions involving metastable states with long lifetime [37], except that intermediate phases of finite polarizations are the ground states at low electric field for composition and temperature in Fig. 4b. We note that the scenario of Lines and Glass, i.e., first-order FE transitions with thermal hysteresis (metastable states), has also been predicted in $PbZrO_3$ nanowires [38], in which FE, pinched, and AFE loops occur with increasing lateral size; however, the transitions appear to be abrupt due to the lack of intermediate bridging phases.

Let us also compare the electric pinched loop in BNFO with the magnetic "pinched" loop observed in SmCo/(Co/Gd) multilayers in Ref. [16]. Both types of loops share one similarity, i.e., at zero electric/magnetic field the antiferro- and ferro-electric/magnetic vectors are both non-zero. However, these two loops also present some significant differences. In particular, the magnetic dipoles lying inside subsequent layers along the stacking direction always couple antiferromagnetically in SmCo/(Co/Gd), whereas in BNFO the in-plane electric dipoles can be (nearly) parallel or antiparallel to each other between different (001)-layers, as evidenced in Fig. 3c. Moreover, "only" the relative magnitude of the magnetic dipoles of the different multilayers varies during the switching in SmCo/(Co/Gd), that is the overall structure remains the same. On the other hand, the system changes of crystallographic structure (from FE *R*3*c* to various intermediate complex structures, as indicated in Fig 4b) during the pinched loop of BNFO, which involves not only a change in dipole moments but also in oxygen octahedral tiltings.

In summary, our study shows that the pinched hysteresis loops in systems possessing electric dipoles can also be intrinsic in nature, as as alluded in Ref. [13] and as similar to the FE and AFE loops, and differ from that found in ferrimagnetic materials. The "electrical" pinched loops are likely to occur in morphotropic phase boundaries for which FE and AFE phases are very close to each other in energy (therefore favoring the emergence of complex inhomogenous states bridging the FE and AFE phases). The present work further suggests that pinched double loops may also be expected to occur in the so-called hybrid improper ferroelectrics, because these latter systems possess a small but finite polarization coexisting with larger anti-polar amplitudes [39–41], as it is the case for some presently investigated complex

phases. We therefore hope that it deepens the current understanding of the fundamentally and technologically-important topics of hysteresis loops, switching and ferroelectricity/antiferroelectricity, in particular that large piezoelectric response can be expected when pinched loop occurs [13, 14]..

This work is financially supported by the Department of Energy, Office of Basic Energy Sciences, under contract ER-46612 (B.X. and L.B.).

* Author to whom correspondence should be addressed. Email address: xubin.physics@gmail.com

[1] J. F. Scott, Science **315**, 954 (2007).
[2] J. F. Scott, *Ferroelectric memories*, Vol. 3 (Springer, 2000).
[3] K. M. Rabe, *Functional Metal Oxides*, edited by S. B. Ogale, T. V. Venkatesan, and B. M. (Wiley, 2013) also available in http://www.physics.rutgers.edu/karin.
[4] H. Liu and B. Dkhil, Z. Kristallogr. **226**, 163 (2011).
[5] X. Hao, J. Adv. Dielect. **03**, 1330001 (2013).
[6] M. H. Park, H. J. Kim, Y. J. Kim, T. Moon, K. D. Kim, and C. S. Hwang, Adv. Energy Mater. **4**, 1400610 (2014).
[7] B. Peng, Q. Zhang, X. Li, T. Sun, H. Fan, S. Ke, M. Ye, Y. Wang, W. Lu, H. Niu, J. F. Scott, X. Zeng, and H. Huang, Adv. Electron. Mater. **1**, 1500052 (2015).
[8] N. Srivastava and G. J. Weng, J. Appl. Phys. **99**, 054103 (2006).
[9] T. Rojac, S. Drnovsek, A. Bencan, B. Malic, and D. Damjanovic, Phys. Rev. B **93**, 014102 (2016).
[10] T. Rojac, M. Kosec, B. Budic, N. Setter, and D. Damjanovic, J. Appl. Phys. **108**, 074107 (2010).
[11] C. Cochard, X. Bril, O. Guedes, and P.-E. Janolin, J. Electron. Mater. **45**, 6005 (2016).
[12] T. Granzow, E. Suvaci, H. Kungl, and M. J. Hoffmann, Appl. Phys. Lett. **89**, 262908 (2006).
[13] Y. Kitanaka, K. Hirano, M. Ogino, Y. Noguchi, M. Miyayama, C. Moriyoshi, and Y. Kuroiwa, Sci. Rep. **6**, 32216 (2016).
[14] D. Kan, L. Pálová, V. Anbusathaiah, C. J. Cheng, S. Fujino, V. Nagarajan, K. M. Rabe, and I. Takeuchi, Adv. Funct. Mater. **20**, 1108 (2010).
[15] D. Kan, V. Anbusathaiah, and I. Takeuchi, Adv. Mater. **23**, 1765 (2011).
[16] S. Demirtas, M. R. Hossu, M. Arikan, A. R. Koymen, and M. B. Salamon, Phys. Rev. B **76**, 214430 (2007).
[17] C.-J. Cheng, D. Kan, S.-H. Lim, W. R. McKenzie, P. R. Munroe, L. G. Salamanca-Riba, R. L. Withers, I. Takeuchi, and V. Nagarajan, Phys. Rev. B **80**, 014109 (2009).
[18] C.-J. Cheng, D. Kan, V. Anbusathaiah, I. Takeuchi, and V. Nagarajan, Appl. Phys. Lett. **97**, 212905 (2010).
[19] S. Emery, C.-J. Cheng, D. Kan, F. Rueckert, S. Alpay, V. Nagarajan, I. Takeuchi, and B. Wells, Appl. Phys. Lett. **97**, 152902 (2010).
[20] I. Levin, S. Karimi, V. Provenzano, C. L. Dennis, H. Wu, T. P. Comyn, T. J. Stevenson, R. I. Smith, and I. M. Reaney, Phys. Rev. B **81**, 020103 (2010).
[21] A. Y. Borisevich, E. Eliseev, A. Morozovska, C.-J. Cheng, J.-Y. Lin, Y.-H. Chu, D. Kan, I. Takeuchi, V. Nagarajan, and S. V. Kalinin, Nat. Commun. **3**, 775 (2012).
[22] B. Xu, D. Wang, J. Íñiguez, and L. Bellaiche, Advanced Functional Materials **25**, 552 (2015).
[23] S. Prosandeev, D. Wang, W. Ren, J. Íñiguez, and L. Bellaiche, Adv. Funct. Mater. **23**, 234 (2013).
[24] S. Karimi, I. Reaney, Y. Han, J. Pokorny, and I. Sterianou, J. Mater. Sci. **44**, 5102 (2009).
[25] I. Levin, M. Tucker, H. Wu, V. Provenzano, C. Dennis, S. Karimi, T. Comyn, T. Stevenson, R. Smith, and I. Reaney, Chemistry of Materials **23**, 2166 (2011).
[26] W. Zhong, D. Vanderbilt, and K. M. Rabe, Phys. Rev. Lett. **73**, 1861 (1994).
[27] W. Zhong, D. Vanderbilt, and K. M. Rabe, Phys. Rev. B **52**, 6301 (1995).
[28] I. A. Kornev, L. Bellaiche, P.-E. Janolin, B. Dkhil, and E. Suard, Phys. Rev. Lett. **97**, 157601 (2006).
[29] See Supplemental Material for more details about the computational method and effect to the pinched loop by using larger simulation supercell.
[30] A. Glazer, Acta Crystallographica Section B: Structural Crystallography and Crystal Chemistry **28**, 3384 (1972).
[31] J. Buhot, C. Toulouse, Y. Gallais, A. Sacuto, R. de Sousa, D. Wang, L. Bellaiche, M. Bibes, A. Barthélémy, A. Forget, D. Colson, M. Cazayous, and M.-A. Measson, Phys. Rev. Lett. **115**, 267204 (2015).
[32] K. Momma and F. Izumi, J. Appl. Crystallogr. **44**, 1272 (2011).
[33] I. A. Kornev and L. Bellaiche, Phys. Rev. B **79**, 100105 (2009).
[34] S. Fujino, M. Murakami, V. Anbusathaiah, S.-H. Lim, V. Nagarajan, C. Fennie, M. Wuttig, L. Salamanca-Riba, and I. Takeuchi, Appl. Phys. Lett. **92**, 202904 (2008).
[35] B. N. Rao, D. K. Khatua, R. Garg, A. Senyshyn, and R. Ranjan, Phys. Rev. B **91**, 214116 (2015).
[36] O. Diéguez, P. Aguado-Puente, J. Junquera, and J. Íñiguez, Phys. Rev. B **87**, 024102 (2013).
[37] M. E. Lines and A. M. Glass, *Principles and applications of ferroelectrics and related materials* (Oxford university press, 1977).
[38] R. Herchig, B. Mani, S. Lisenkov, and I. Ponomareva, Comput. Mater. Sci. **117**, 468 (2016).
[39] J. M. Rondinelli and C. J. Fennie, Adv. Mater. **24**, 1961 (2012).
[40] A. T. Mulder, N. A. Benedek, J. M. Rondinelli, and C. J. Fennie, Adv. Funct. Mater. **23**, 4810 (2013).
[41] B. Xu, D. Wang, H. J. Zhao, J. Íñiguez, X. M. Chen, and L. Bellaiche, Advanced Functional Materials **25**, 3626 (2015).